Journal of Alloys and Compounds 506 (2010) 77–84

Contents lists available at ScienceDirect

Journal of Alloys and Compounds

journal homepage: www.elsevier.com/locate/jallcom

Microstructural characteristics and degradation mechanism of the NiCrAlY/CrN/DSM11 system during thermal exposure at 1100 °C

Weizhou Li[a,b,*], Yueqiao Li[a], Chao Sun[b], Zhiliu Hu[a], Tianquan Liang[a], Wuquan Lai[a]

[a] School of Materials Science and Engineering, Guangxi University, 100 Daxue Road, Nanning 530004, PR China
[b] State Key Lab for Corrosion and Protection, Institute of Metal Research, Chinese Academy of Sciences, Shenyang 110016, PR China

ARTICLE INFO

Article history:
Received 7 December 2009
Received in revised form 26 June 2010
Accepted 30 June 2010
Available online 7 July 2010

Keywords:
Coatings
Diffusion barrier
Interdiffusion
Oxidation-resistance
Microstructure

ABSTRACT

To limit the elemental interdiffusion, a CrN diffusion barrier was introduced into the interface of NiCrAlY overlayer and DSM11 substrate. During vacuum heat treatment and thermal exposure, the single and continuous CrN barrier layer was first changed to the multilayer structure and then to the Ti-rich interlayer. With the gradual loss of continuity in the diffusion barrier, the elemental interdiffusion was accelerated. Due to the interdiffusion, the transformation of β-NiAl → γ′-Ni_3Al → γ-Ni and the low Al level occurred in the overlayer. The phase transformation of metastable θ-Al_2O_3 to stable α and the accelerated elemental interdiffusion affected the integrity of the surface scales. After 100 h exposure at 1100 °C, the Al element was insufficient and the duplex coatings were degraded.

1. Introduction

MCrAlY (M = Ni and/or Co) coatings, with good balance between oxidation-resistance, corrosion resistance and ductility, are widely utilized on blades and other high temperature components in gas turbine engines both as standalone coatings and as bond coats for thermal barrier coating systems (TBCs) [1–3]. During long-term service at high temperature atmosphere, the protection effect of MCrAlY coatings is impaired by elemental interdiffusion between the coatings and the substrate [4–6]. It is described that the interdiffusion accelerates the protective surface scales spalling and makes the continuous scales not regenerated because of the depletion of Cr and Al elements. Developing a diffusion barrier as an interlayer can effectively inhibit the elemental interdiffusion, thus markedly prolong the service life of the MCrAlY coatings [7].

With the introduction of diffusion barrier into the coating/substrate interface, two major questions are raised that whether the interfacial bonding strength of the coating system is markedly weakened and the oxidation-resistance of the coatings can be improved [5,7]. With the aid of tensile adhesion test, it is found that the interfacial adhesion is about 70 MPa in the annealed MCrAlY/CrN/DSM11 system (herein CrN is as a diffusion barrier), better than that with CrON diffusion barriers. After thermal exposure, the interfacial adhesion of the coating system with the CrN diffusion barrier is further improved to above 80 MPa, which is attributed to the replacement of CrN by TiN in the diffusion barrier [8,9]. However, due to the destruction of continuous CrN barrier layer, the barrier effectiveness will inevitably change and thus the oxidation-resistance will be affected. In this paper, a CrN diffusion barrier was deposited into the NiCrAlY/DSM11 interface by arc ion plating (AIP). By investigating the microstructural evolution of the NiCrAlY/CrN duplex coatings during thermal exposure at 1100 °C, the oxidation-resistance and the degradation mechanism of the coatings were discussed.

2. Experimental

2.1. Preparation of coatings

A Ni-based superalloy DSM11 was used as the substrate, whose nominal composition (wt.%) is: Cr 14.0; Co 9.5; W 3.8; Mo 1.5; Ta 2.8; Al 3.0; Ti 4.9; B 0.015; C 0.10; the balanced nickel. Rectangular specimens with dimensions 15 × 10 × 2 mm^3 were ground down to 1000-grit SiC paper, grit-blasted in wet atmosphere (200-mesh glass ball), and then ultrasonically rinsed in ethanol and dried in air. Before deposition, the substrate was ion cleaned with Ar^+ for 5 min at a negative bias of −800 in the AIP system. The diffusion barrier was deposited with a pure Cr target in a nitrogen pressure of 0.6 Pa. The NiCrAlY overlayer was deposited with a Ni–23Cr–10Al–0.2Y (wt.%) alloy target in an Ar atmosphere of 0.3 Pa. The deposition time was controlled 30 min for CrN diffusion barrier and 360 min for NiCrAlY overlayer, respectively. During deposition, the arc current was 65–75 A and the negative bias voltage was 150–250 V. After deposition, the specimens were annealed at 600 °C for 20 h, 900 °C for 4 h in a vacuum furnace at a heating rate of 7 °C/min for the stress release and subsequently cooled down to room temperature.

2.2. Oxidation and microstructure analysis

The isothermal oxidation tests were conducted in static air at 1100 °C for 100 h. The specimens were placed in alumina crucibles so that the total mass change

* Corresponding author. Tel.: +86 771 3270152; fax: +86 771 3270152.
E-mail address: wz-li@hotmail.com (W. Li).

0925-8388/$ – see front matter © 2010 Elsevier B.V. All rights reserved.
doi:10.1016/j.jallcom.2010.06.168

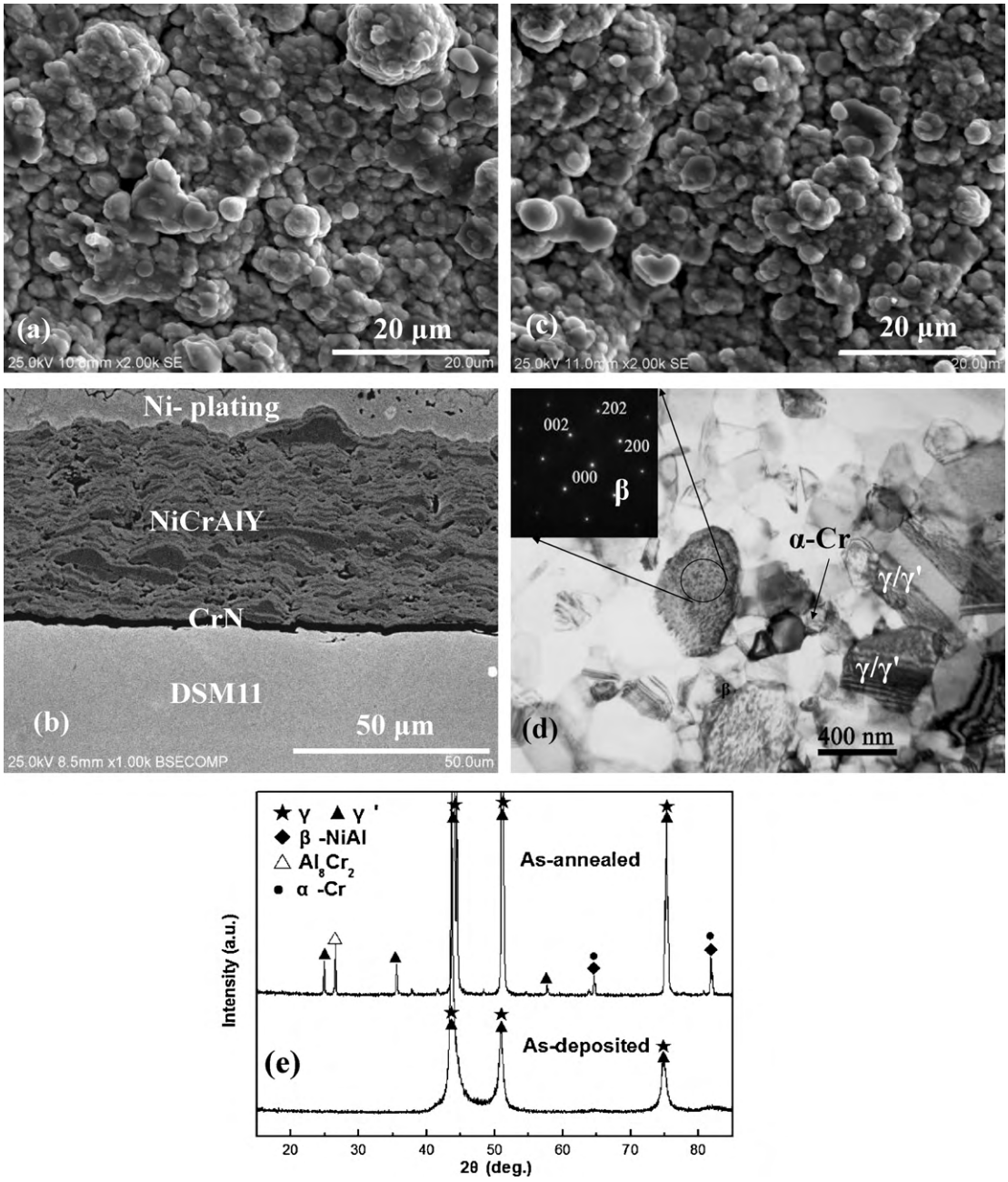

Fig. 1. Surface morphologies (a and c), cross-sectional image (b), TEM micrograph of the overlayer (d) and XRD patterns (e) of the as-deposited (a and b) and annealed (c and d) samples.

including spalled oxides could be obtained. Prior to the oxidation tests, these alumina crucibles were heated at 1200 °C until no mass change was observed. The mass change of the specimens with crucibles was measured discontinuously by interrupting the oxidation process. Three specimens were simultaneously tested and the mean values of the mass change were used. The sensitivity of the balance used was 10^{-5} g. Some specimens exposed for 10 and 50 h were taken out for subsequent analysis.

The phase constituents of the coatings before and after oxidation were identified by X-ray diffraction (XRD, Cu Kα). The identification of Al_2O_3 phase in the surface oxides was done by photo-stimulated luminescence spectrum (PSLS). The excitation source was a Nd: YVO_4 DPSS laser with photon wavelength of 532 nm. The incident laser beam was focused onto the specimen surface with a laser spot of approximately 2.1 μm in diameter. The average residual stress in the scales was evaluated from the PSLS peak shift of 20 different places. The annealed Al_2O_3 powders were taken as reference sample. The microstructural observation of the coating systems was conducted by scanning electron microscope (SEM) and transmission electron microscope (TEM). The TEM samples were prepared by conventional procedure, including polishing to approximately 40 μm thickness from cross-section, followed by cutting 3 mm diameter discs, dimpling to 20 μm and finally ion milling. The crystal structure of the grain was analyzed by selected-area electron diffraction (SAD). The energy-dispersive spectrometer (EDS) with a window-section or line scanning mode was used to analyze the average chemical composition of the selected-area or the element distribution along the cross-sectional sample.

3. Results and discussion

3.1. Coating microstructure

Fig. 1 shows the SEM and TEM images and XRD patterns of the coating system before and after vacuum heat treatment. From the surface image (Fig. 1(a)), it is found that the as-deposited NiCrAlY coatings are rather rough with the constitution of spherical and semi-spherical macro particles. The cross-sectional image indicates that the overlayer possesses an inhomogeneous and lamellar structure (Fig. 1(b)). After vacuum heat treatment, the coating

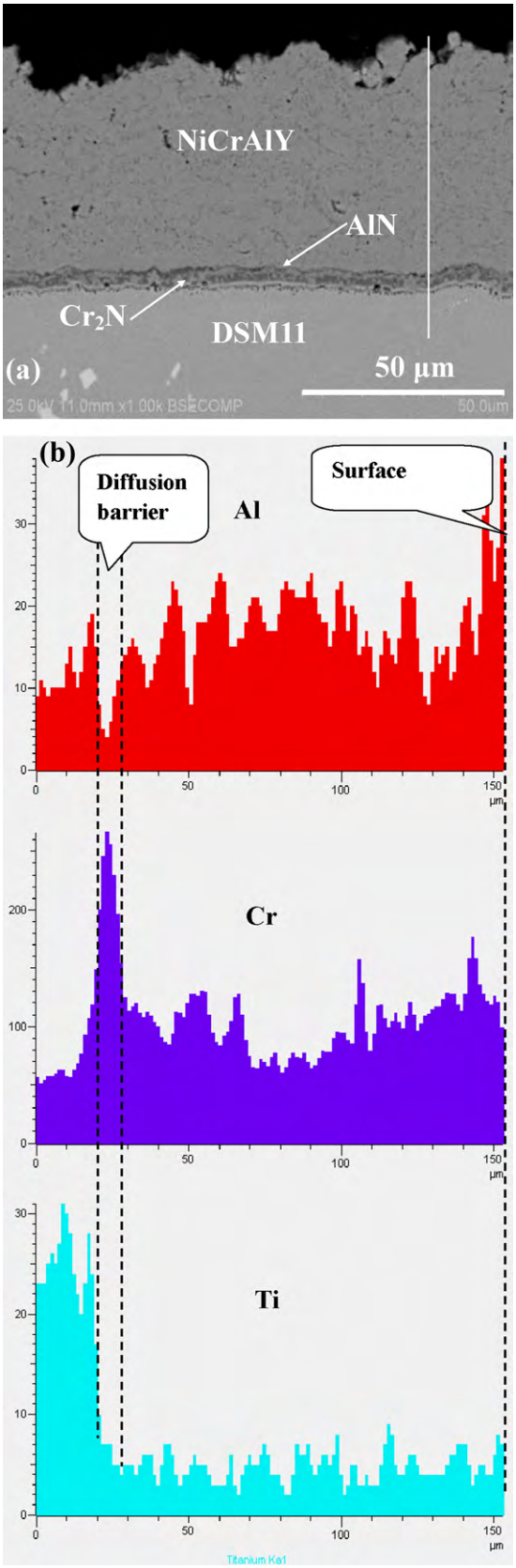

Fig. 2. Cross-sectional SEM image (a) and EDS line scanning (b) of the annealed sample.

surface morphologies were altered little (Fig. 1(c)). The TEM micrograph (Fig. 1(d)) illuminates that in addition to the typical twinned γ-Ni/γ′-Ni_3Al gains, β-NiAl and α-Cr grains are present in the annealed NiCrAlY coatings. The XRD patterns (Fig. 1(e)) indicates that the γ-Ni and γ′-Ni_3Al exist by amorphous or nano-crystalline phases in the as-deposited NiCrAlY coatings with the broad diffraction peaks [10], and β-NiAl and α-Cr were precipitated in the overlayer during vacuum heat treatment.

Fig. 2 shows the cross-sectional SEM image and EDS line scanning of the annealed coating sample. Compared with the as-deposited sample, the annealed overlayer is homogeneous and dense, and the CrN diffusion barrier was changed into the multilayer structure (Fig. 2(a)). The EDS line scanning indicates that Cr-rich phase is concentrated in the center of diffusion barrier and Al-rich phase is formed at the overlayer/DB interface. It was confirmed that the Cr-rich phase was Cr_2N, which was transformed from CrN and the Al-rich phase was AlN due to the replacement reaction of inward-diffusion Al with CrN during vacuum heat treatment [9]. From the EDS line scanning results, it can also be observed that the Al and Cr elements are distributed non-uniformly in the overlayer and most of Ti was detected in the substrate. The content of Al, Cr and Ti in the overlayer is 7.49, 27.13 and 0.05 at.%, respectively.

3.2. Oxidation behavior of the coating systems

Fig. 3 represents the curves of mass gain vs. exposed time for the NiCrAlY/DSM11 and NiCrAlY/CrN/DSM11 samples exposed at 1100 °C for 100 h. In the first 30 h, the NiCrAlY/DSM11 sample and the NiCrAlY/CrN/DSM11 sample present a comparative mass gain. Thereafter, they exhibit a similar trend, but the single coating sample has a slightly faster mass gain. After 100 h exposure, the mass gain for the NiCrAlY/DSM11 sample is about 2.3045 mg/cm^2 and it is 1.2687 mg/cm^2 for the NiCrAlY/CrN/DSM11 sample. The observation during interrupted thermal exposure revealed that apparent scales spalled from the surface of NiCrAlY/DSM11 sample after 70 h, while only slight spallation was detected on the NiCrAlY/CrN/DSM11 sample after 100 h. Thus, it can be concluded that the introduction of CrN diffusion barrier can improve the oxidation-resistance of coating system.

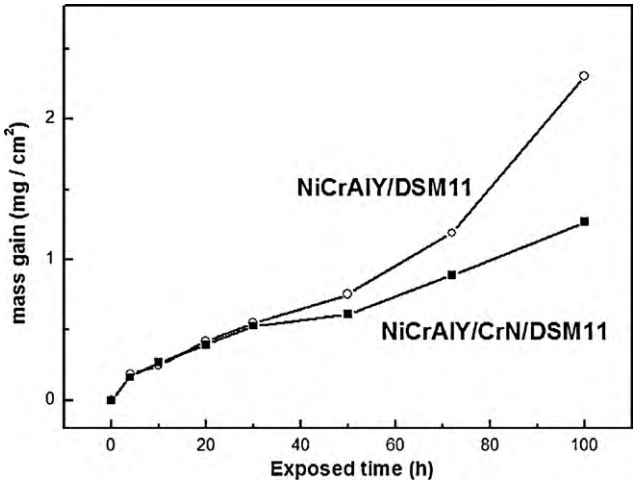

Fig. 3. Dependence of mass gain on time for the NiCrAlY/CrN/DSM11 and NiCrAlY/DSM11samples exposed at 1100 °C for 100 h.

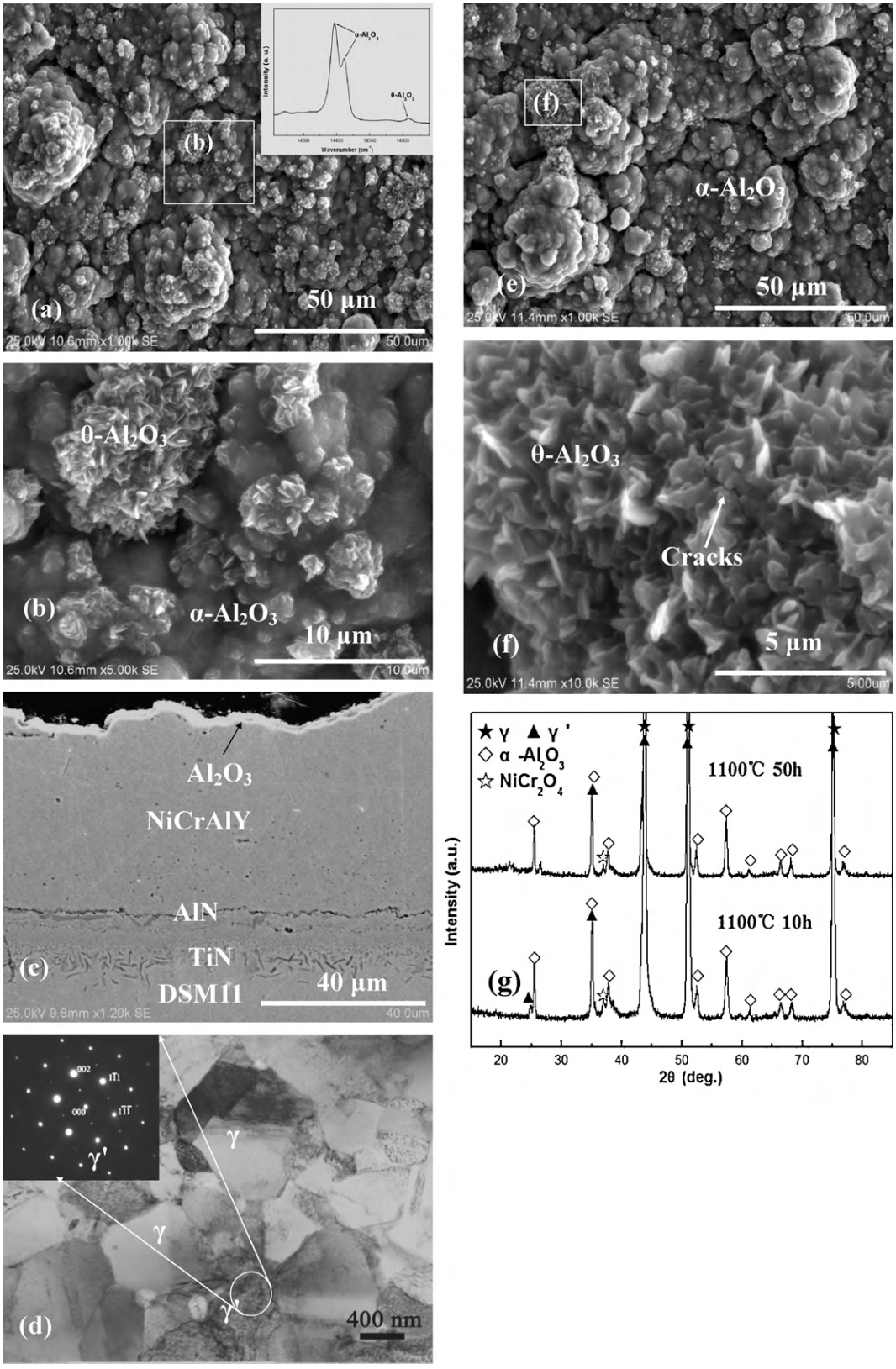

Fig. 4. Surface morphologies (a, b, e and f), cross-sectional image (c), TEM micrograph of the overlayer (d) and XRD patterns (g) of the samples exposed at 1100 °C for 10 h (a–d) and 50 h (e and f). The inset in (a) shows the typical PSLS peaks for the scales. The inset SAD patterns in (d) indicates the presence of γ′ grains. (b and f) The magnified images of the selected zones in (a) and (e), respectively.

3.3. Microstructural evolution

Fig. 4 shows the SEM and TEM morphologies and XRD patterns of the samples exposed at 1100 °C for 10 and 50 h. As it is observed, two representative oxides are present on the sample surface: needle-like θ-Al_2O_3 [11] and scale-like α-Al_2O_3 (Fig. 4(a)). The coexistence of θ and α phase in the surface scales is also confirmed by the PSLS curve inserted in the Fig. 4(a). From the peak shift of α-Al_2O_3 [12], it was estimated to about −1 GPa of residual stress present in the sample scales. The magnified image shows that θ-Al_2O_3 scales are embedded into the α-Al_2O_3 scales (Fig. 4(b)). From the cross-sectional image (Fig. 4(c)), it is found that thin alumina scales are adhered to the coating surface. The upper interface of the diffusion barrier is continuous, and the downside is predominated by discontinuous Ti-rich particles. The EDS analysis indicates that only about 0.09 at.% Ti was detected in the overlayer, and the content of Al and Cr is 6.46 and 26.15 at.%, respectively. The TEM micrograph (Fig. 4(d)) illuminates that coarsened γ and γ′ grains are presented in the 10 h exposed overlayer. After 50 h exposure, the content of needle-like θ-Al_2O_3 on the coating surface decreased (Fig. 4(e)), which is the result from the phase transformation of metastable θ-Al_2O_3 to the thermodynamically stable α-Al_2O_3. The magnified image reveals that micro-cracks are present in the needle-like θ-Al_2O_3 grains (Fig. 4(f)). The XRD patterns show that the main oxidation product of the coating samples is α-Al_2O_3 (Fig. 4(g)). In addition, with the extension of exposure time form 10 h to 50 h, the diffraction peaks of γ′ phase were reduced little in the quantity.

Fig. 5 shows the SEM and TEM images, XRD patterns and the EDS line scanning of the samples exposed at 1100 °C for 100 h. No needle-like θ-Al_2O_3 is observed on the sample surface, but cracks and spallation zone with a small area were formed (Fig. 5(a)). The magnified image shows that the spallation zone exhibits a porous structure (Fig. 5(b)). The EDS detection indicates that the content of Al, Cr, Ti, Ni and O is 2.53, 24.32, 4.56, 18.07 and 48.07 at.%, respectively, and thus it is deemed the formation of $NiCr_2O_4$ and TiO_2 in the spallation zone. The TEM micrograph displays that the γ grains were grown to about 1 μm in size in the overlayer (Fig. 5(d)). Compared with the 50 h exposed sample, the phase compositions of the 100 h exposed sample changed little, as demonstrated in Fig. 5(d). From the cross-sectional image (Fig. 5(e)), it is observed that the diffusion barrier layer was fully replaced by the palpus-like TiN particles. The EDS line scanning shows that the majority of Ti is detected in the DB zone, and Al and O are the main elements of the surface scales (Fig. 5(f)). The quantitive element analysis represents that the mean content of Al and Cr was reduced to 4.74 and 22.86 at.%, respectively, and Ti increased to 1.55 at.% in the overlayer. Thus, it can be concluded that with the destruction of continuous diffusion barrier the elemental interdiffusion between the coatings and the substrate became intensive.

In comparison with the coating sample with a diffusion barrier, the integrity of the surface scales and the elemental interdiffusion in the single coating/substrate sample were different, as displayed in Fig. 6. On the coating surface (Fig. 6(a)), a large area of spallation zone was formed. After the scales spalling, the porous mixed oxides of $NiCr_2O_4$ and TiO_2 emerged (Fig. 6(b)). The EDS analysis indicates that a higher content of Ti, about 6.62 at.% is present in the spallation zone. The formation of TiO_2 can be confirmed by the XRD detection (Fig. 6(c)). From the XRD patterns, it is also found that the peaks of $NiCr_2O_4$ spinels were augmented and intensified, in contrast to the XRD result of the 100 h exposed duplex coating sample (Fig. 5(d)). The cross-sectional image of the single coating sample displays the formation of thick mixed-oxide scales on the coating surface, with distinct cracks in it (Fig. 6(d)). Besides, many interdiffusion holes are also observed in the overlayer. The EDS line scanning shows that in addition to the enrichment of Ti in the coating zone adjacent to the surface scales, a little higher content of Ti was detected in the surface scales (Fig. 6(e)). The quantitive EDS analysis implies a significant decrease of Al and Cr content in the overlayer up to 2.62 and 21.13 at.%, respectively. Thus, it can be concluded that the single coating system suffered a more serious oxidation attack and more intensive elemental interdiffusion than the duplex coating system during thermal exposure.

3.4. Oxidation-resistance and degradation of the coatings

As it is well known, the oxidation-resistance of MCrAlY coatings mainly depends on the formation of protective surface scales [3]. The exclusive growth of continuous, dense and thermal-stable α-Al_2O_3 scales is an ideal outcome. The long-term effectiveness of the coatings is deeply affected by the content of Al and Cr elements in the coatings. A low Al level makes it difficult to form and regenerate continuous and protective alumina scales on the coating surface. The presence of Cr in the coatings can decrease the concentration of Al required to establish the external Al_2O_3 scales according to the third element effect [13].

When MCrAlY coatings are exposed to high temperature atmosphere, NiO, Cr_2O_3 and Al_2O_3 first form on the surface according to the following reactions:

$$\gamma\text{-Ni} + [O] \rightarrow NiO$$

$$2\gamma'\text{-}Ni_3Al + 9[O] \rightarrow 6NiO + Al_2O_3$$

$$2\beta\text{-NiAl} + 5[O] \rightarrow 2NiO + Al_2O_3$$

$$2\alpha\text{-Cr} + 3[O] \rightarrow Cr_2O_3$$

Then, NiO will react with Cr_2O_3 to form $NiCr_2O_4$. At the initial oxidation stage, it is deemed that the formation of θ-Al_2O_3 and α-Al_2O_3 occurs simultaneously [11,14,15]. The fast-growing of θ-Al_2O_3 can explain the higher oxidation mass gains of the coating samples. During the sequent exposure, the metastable θ-Al_2O_3 will transform to the stable and slow-growing α phase, and which often causes the scales crack due to the remarkable volume contraction of θ to α [11].

Meanwhile, the inward-diffusion Al occurs under the drive of chemical potential difference, which leads to the formation of AlN due to a lower formation free energy of AlN than that of CrN or Cr_2N. Together with the outward-diffusion of Al and Cr to thicken the surface scales [16], the content of Al in the overlayer decreases and the following transformation takes place:

$$3\beta\text{-NiAl} \rightarrow \gamma'\text{-}Ni_3Al + 2[Al]$$

During the interrupted oxidation tests, the surface scales are prone to spall off from the coatings due to the remarkable different coefficients of thermal expansion (CTEs) between the ceramic oxides and the metal coatings, in particularly when the coating samples are cooled from high temperature to the room temperature. Reheated to high temperature, new oxide scales are built up. In this case, incessant Al and Cr elements in the overlayer migrate outwards for maintaining the continuous surface scales, and the transformation of γ′ to γ occurs,

$$2\gamma'\text{-}Ni_3Al \rightarrow 6\gamma\text{-Ni} + 2[Al]$$

Practically, the formation of γ is beneficial to the transformation of β to γ′.

Otherwise, the alloying elements from the substrate also traverse the coating/substrate interface and enter the overlayer. It is reported that the diffusion of Ti element has a deleterious influence on the stability of the surface scales [17,18]. After the formation of

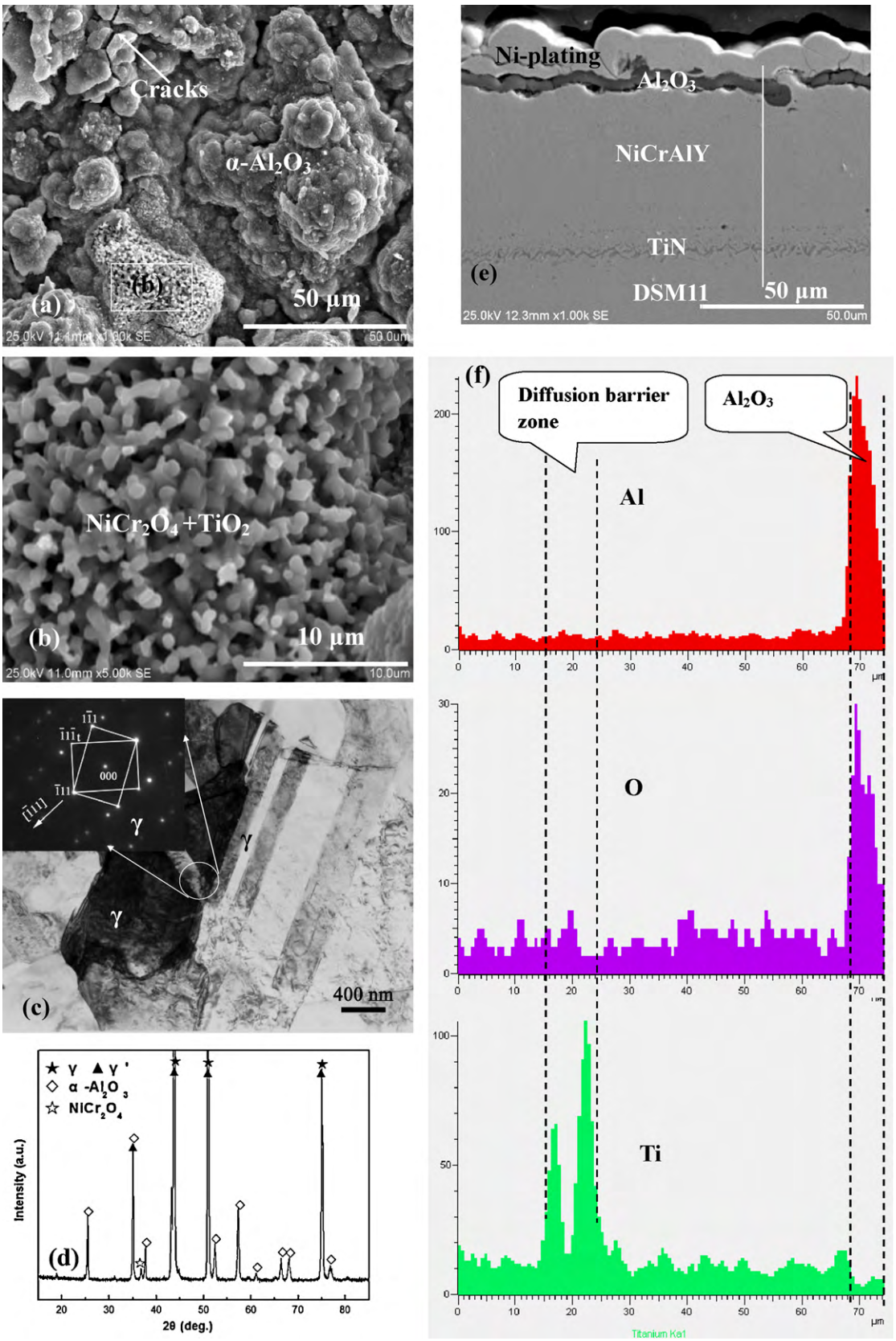

Fig. 5. Surface morphologies (a and b), TEM micrograph of the overlayer (c), XRD patterns (d), cross-sectional image (e) and EDS line scanning (f) of the samples exposed at 1100 °C for 100 h. The inset SAD patterns in (c) shows the twinned γ grains. (b) is the magnified image of the selected zone in (a).

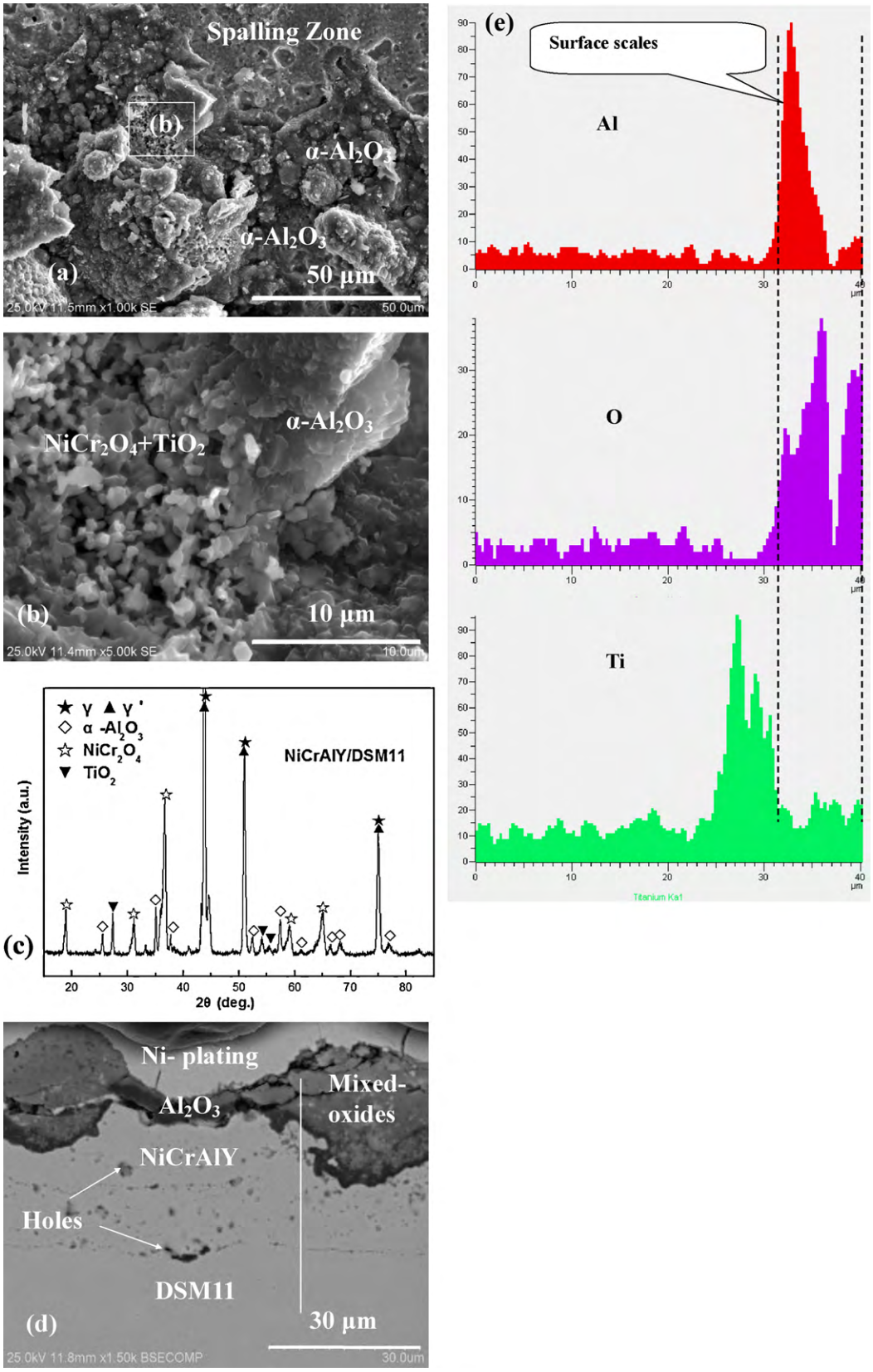

Fig. 6. Surface morphologies (a and b), XRD patterns (c), cross-sectional image (d) and EDS line scanning (e) of the single NiCrAlY coating sample exposed at 1100 °C for 100 h. (b) The magnified image of the selected zone in (a).

TiO_2 at the scales/coating, a high interfacial stress will be introduced and thus the resistance of the scales to spallation is lowered. In the present work, CrN diffusion barrier was arranged into the coating system to decrease the interdiffusion. During the initial thermal exposure, the outward-diffusion Ti was inhibited and the surface scales were adhered to the coatings. Also, the inward-migration of Al and Cr was reduced to some degree. After the scale spallation, the element reservoir in the overlayer ensured sufficient Al content required for the healing of continuous surface scales. However, with the increase of thermal exposure time, the CrN barrier layer gradually lost its continuity to become a TiN-dispersed interlayer, and thereafter the alloying elements could diffuse across the barrier layer more easily. With the repeated loss of the scales and the interdiffusion, the residual Al level was reduced to the point where the generation became impossible. Due to the serious scale spallation and the Al depletion, the surface scales became discontinuous and could not be healed, hereafter the degradation of the coating system occurred.

4. Conclusions

With the introduction of CrN diffusion barrier, the elemental interdiffusion of NiCrAlY overlayer and DSM11 substrate was reduced and therefore the oxidation-resistance of the duplex coating sample was improved to some degree. However, due to the destruction of the continuity in the barrier layer, the interdiffusion was accelerated and the protection effect of the surface scales was lowered. The transformation of θ-Al_2O_3 to α-Al_2O_3 and the outward-diffusion of Ti element affected the integrity of the surface scales. The outward and inward-diffusion depleted Al and Cr elements, and meanwhile a series of phase transformation took place in the overlayer. With the depletion of the Al and Cr element, the NiCrAlY coatings were degraded gradually.

Acknowledgments

This work was supported by Guangxi Science Foundation (Grant nos. 2010GXNSFD013006 and 0731013), Scientific Research Foundation of Guangxi University (Grant no. XBZ090331) and Opening Foundation of Key Laboratory of New Processing Technology for Nonferrous Metal and Materials of Ministry of Education (Grant no. GXKFJ09-22), which is gratefully acknowledged.

References

[1] N.P. Padture, M. Gell, E.H. Jordan, Science 296 (2002) 280–284.
[2] Z.H. Xu, R.D. Mu, L.M. He, X.Q. Cao, J. Alloys Compd. 466 (2008) 471–478.
[3] J.R. Nicholls, MRS Bull. 28 (2003) 659–670.
[4] Q.M. Wang, K. Zhang, J. Gong, Y.Y. Cui, C. Sun, L.S. Wen, Acta Mater. 55 (2007) 1427–1439.
[5] O. Knotek, E. Lugscheider, F. Löffler, W. Beele, Surf. Coat. Technol. 68/69 (1994) 22–26.
[6] O. Knotek, F. Löffler, W. Beele, Surf. Coat. Technol. 61 (1993) 6–13.
[7] Q.M. Wang, Y.N. Wu, M.H. Guo, P.L. Ke, C. Sun, L.S. Wen, Surf. Coat. Technol. 197 (2005) 68–76.
[8] Y. Yao, W.Z. Li, Q.M. Wang, J. Gong, C. Sun, J.B. Li, Acta Metal. Sin. 44 (2008) 876–882.
[9] W.Z. Li, Q.M. Wang, J. Gong, C. Sun, X. Jiang, Appl. Surf. Sci. 255 (2009) 8190–8193.
[10] C. Sun, Q.M. Wang, Y.J. Tang, Q.F. Guan, J. Gong, L.S. Wen, Acta Metall. Sin. 41 (2005) 1167–1173.
[11] Z.Y. Liu, W. Gao, F.H. Wang, Scripta Mater. 39 (1998) 1497–1502.
[12] R.J. Christensen, D.M. Lipkin, D.R. Clarke, K. Murphy, Appl. Phys. Lett. 69 (1996) 3754–3756.
[13] F.H. Stott, G.C. Wood, J. Stringer, Oxid. Met. 44 (1995) 13–145.
[14] D.M. Lipkin, H. Schaffer, F. Adar, D.R. Clarke, Appl. Phys. Lett. 70 (1997) 2550–2552.
[15] Y.J. Xie, M.C. Wang, J. Alloys Compd. 480 (2009) 454–461.
[16] K.P.R. Reddy, J.L. Smialek, A.R. Cooper, Oxid. Met. 17 (1982) 429–449.
[17] P.S. Liu, K.M. Liang, S.R. Gu, Corros. Sci. 43 (2001) 1217–1226.
[18] B. Wang, A.Y. Wang, C. Sun, R.F. Huang, L.S. Wen, Chin. J. Aeronaut. 14 (2001) 106–111.